NRC Publications Archive
Archives des publications du CNRC

Model testing and performance comparison of plastic and metal tidal turbine rotors

Liu, Pengfei; Bose, Neil; Frost, Rowan; Macfarlane, Gregor; Lilienthal, Tim; Penesis, Irene

This publication could be one of several versions: author's original, accepted manuscript or the publisher's version. / La version de cette publication peut être l'une des suivantes : la version prépublication de l'auteur, la version acceptée du manuscrit ou la version de l'éditeur.
For the publisher's version, please access the DOI link below./ Pour consulter la version de l'éditeur, utilisez le lien DOI ci-dessous.

Publisher's version / Version de l'éditeur:
https://doi.org/10.1016/j.apor.2015.08.002
Applied Ocean Research, 53, pp. 116-124, 2015-08-28

NRC Publications Archive Record / Notice des Archives des publications du CNRC :
https://nrc-publications.canada.ca/eng/view/object/?id=15a02f99-2b14-48ec-aa13-ed0e3c106864
https://publications-cnrc.canada.ca/fra/voir/objet/?id=15a02f99-2b14-48ec-aa13-ed0e3c106864

Access and use of this website and the material on it are subject to the Terms and Conditions set forth at
https://nrc-publications.canada.ca/eng/copyright
READ THESE TERMS AND CONDITIONS CAREFULLY BEFORE USING THIS WEBSITE.

L'accès à ce site Web et l'utilisation de son contenu sont assujettis aux conditions présentées dans le site
https://publications-cnrc.canada.ca/fra/droits
LISEZ CES CONDITIONS ATTENTIVEMENT AVANT D'UTILISER CE SITE WEB.

Questions? Contact the NRC Publications Archive team at
PublicationsArchive-ArchivesPublications@nrc-cnrc.gc.ca. If you wish to email the authors directly, please see the first page of the publication for their contact information.

Vous avez des questions? Nous pouvons vous aider. Pour communiquer directement avec un auteur, consultez la première page de la revue dans laquelle son article a été publié afin de trouver ses coordonnées. Si vous n'arrivez pas à les repérer, communiquez avec nous à PublicationsArchive-ArchivesPublications@nrc-cnrc.gc.ca.

National Research Council Canada
Conseil national de recherches Canada

Model Testing and Performance Comparison of Plastic and Metal Tidal Turbine Rotors

Pengfei Liu[a], Neil Bose[b], Rowan Frost[b], Gregor Macfarlane[b], Tim Lilienthal[b], Irene Penesis[b]

[a] *Ocean, Coastal and River Engineering, National Research Council Canada, 1 Kerwin Place and Arctic Avenue, Box 12093, St. John's, NL, A1B 3T5, Canada*
[b] *Australian Maritime College, University of Tasmania, Maritime Way, Newnham, Tasmania 7248, Australia*

Abstract

Experimental model tests were conducted to predict the performance of two sets of metal and plastic bi-directional tidal turbine rotors. This test program aims to provide reliable and accurate measurement data as references for developers, designers and researchers on both model and full scale. The data set presented in this paper makes available the detailed geometry and motion parameters that are valuable for numerical tools validation. A rotor testing apparatus that was built using an off-the-shelf K&R propeller dynamometer, its configuration, testing set-up, calibration of the apparatus and data acquisition are described. Comparison analysis between the metal and plastic rotors hydrodynamic performance in terms of torque, drag and derived power and drag coefficients are also presented. The results show a substantial decrease in maximum power performance for the plastic ro-

Email addresses: `Pengfei.Liu@nrc-cnrc.gc.ca` (Pengfei Liu), `N.Bose@amc.edu.au` (Neil Bose), `rtfrost@amc.edu.au` (Rowan Frost), `G.Macfarlane@amc.edu.au` (Gregor Macfarlane), `T.Lilienthal@amc.edu.au` (Tim Lilienthal), `I.Penesis@amc.edu.au` (Irene Penesis)

tors — about 40% decrease at a tip speed ratio of around 3.0, compared with rigid metal rotors. The plastic rotors have also a much higher cut-in speed. It showed that materials for rotor models with low rigidity such as polyamide (nylon) produced by selective laser sintering (SLS) systems may substantially under-predict power generation capacity. As a result, they are considered unsuitable for rotor model performance evaluation.
Keywords: metal and plastic rotor testing, bi-directional turbine, HATT, HACT

Nomenclature

Symbol	Description	Units
D	Rotor diameter,	m
R	Rotor radius,	m
A	Area of rotor disk, $A = \pi R^2$	m^2
α_p	Geometric angle of blade section	Rad or deg
α'_v	Resultant angle of inflow velocity with added induced velocity,	Rad or deg
α_o	Angle of zero lift of blade section,	Rad or deg
α_e	Effective angle of attack of blade section,	Rad or deg
$c_{0.7R}$	Blade chord length at $r = 0.7R$	m
n	Rotor shaft speed,revolution per second,	rps
N	Rotor shaft speed,revolution per minute,	RPM
R	Rotor radius,	m
Z	Number of blades	
V_{in}	Tidal inflow speed at rotor disk plane,	m/s

ρ	Fluid density,	kg/m^3
μ	Fluid dynamic viscosity,	$N \cdot s/m^2$
ν	Fluid kinetic viscosity,μ/ρ,	m^2/s
p	Blade pitch,	m
p_D	Blade pitch diameter ratio	
$p_{D_{0.7R}}$	Blade pitch diameter ratio at $r = 0.7R$,	
$V_{resultant}$	$=\sqrt{(0.7R\omega)^2 + V_{in}^2}$, Resultant velocity at $r = 0.7R$,	m/s
V_a	Inflow velocity,	m/s
V_a'	Inflow velocity with added induced velocity,	m/s
V_t	Induced tangential velocity at the rotor disk plane,	m/s
V_x	Induced axial velocity at blade section	m/s
EAR	Rotor disk solidity $EAR = \frac{A_{rotor}}{\pi R^2}$	
TSR	Tip speed ratio $TSR = \frac{2\pi nR}{V_{in}}$	
R_n	Reynolds number, $Rn = \frac{VL}{\nu} = \frac{\sqrt{(0.7R\omega)^2+V_{in}^2)}c_{0.7R}}{\nu}$	
Q	Shaft torque,	$N \cdot m$
T	Thrust or drag on shaft	N
Q_{adj}	Adjusted torque measurement,	$N \cdot m$
$Q_{measured}$	Measured torque,	$N \cdot m$
Q_{tare}	Tare torque,	$N \cdot m$
Q_0	Torque reading at zero torque,	$N \cdot m$
C_t	Rotor thrust/drag coefficient, $C_t = \frac{T}{1/2\rho V_a^2}$	
C_{pow}	Rotor power coefficient, $C_{pow} = \frac{P}{1/2\rho V_a^3 A}$	

1. Introduction

With the rapid development of renewable energy turbine science and technologies, more and more horizontal axis turbine rotors were tested in both model and full scale, to assess their power coefficient. Publications providing a complete suite of geometry and motion data that could be conveniently and effectively used as a methodical series, are rarely found. The best examples existing include a set of measurement data from a full scale trial of a wind turbine rotor [5], a set of experimental testing data for an unidirectional-bladed tidal turbine rotor model with controllable pitch [4], and a full suite of measured data, detailed geometric and motion parameters along with a detailed description of the testing apparatus in a recent work [13]. These have effectively provided for the demand for the availability of physical measurement data for numerical code validation, research and development and industrial design reference.

Tidal currents in terms of ebb and flood tides, are bi-directional. Horizontal axis tidal turbines need to be designed to operate in both directions. As summarized in a recent work [12], there are three basic configurations for tidal turbines to work in bi-directional currents: 1) An unidirectional turbine which "weather vanes" (at about 180°) so that it always faces the current. This kind of turbines uses unidirectional blade; 2) A bi-directional turbine with unidirectional blade section achieved by reversing blade pitch angle (180°); and 3) A bi-directional rotor with fully symmetrical blade section that operates identically in both tidal flow directions with shaft rotating in opposing directions. Each of these individual configurations has advantages and disadvantages; for example, the bi-directional blade of the 3rd configuration will result in a reduced hydrodynamic performance but it saves the mechanical and electronic control needed for either alternating the orientation of the turbine alternating the pitch of the blades at about 180°. For the 3rd tidal turbine configuration, a comprehensive numerical simulation and optimization for horizontal axis turbines operating under the tidal flow conditions of Minus passage, the Bay of Fundy was completed with emphases on hydrodynamic performance [12] and optimization for structural strength and integrity [15], under a research project funded by Natural Resources Canada (NRCan). As a result of over 15,000 data runs and analysis in the simulation and optimization processes completed [12] using a time-domain and multiple-body panel method, 10 rotors were initially recommended for further experimental model testing. For the rotor series testing program [14], 10 plastic rotors and 7 metal rotor models were made. Hydrodynamic characteristics of the 7 metal rotors were presented in a recent work [13].

The use of plastic materials for rotor model testing has great advantages in terms of meeting client requirements to minimize cost and manufacture time. For example, depending on roughness and manufacture accuracy requirement, the cost of the plastic rotor model is approximately $1/10th$ of the aluminium rotor with the same size ($200 versus $2,000) and about $1/25th$ of the stainless steel rotor models ($200 versus $5,000). The time required to manufacture a plastic rotor via a 3D printer is about $1/10th$ of the aluminium one via a CNC machine (1 hours versus 10 hours). In the past few decades, computer-aided manufacturing of rotor models using CNC and 3D printing technology has advanced dramatically, along with the lighter and much lower cost materials (less than 10% total cost compared with CNC metal rotors).

While rotor models produced by 3D printing for demonstration and showcase become more and more popular, there have been wide instances and examples of using 3D printers to produce rotors for hydrodynamic performance model testing, especially for self-propulsion tests, for example, at co-authors institutions, National Research Council Canada and University of Tasmania, Australia and their domestic maritime research communities.

Depending on particular 3D printers, materials used for rotor model production have a wide variety of strength properties. Hydrodynamic performance of rotors made of the sintered material similar to Nylon 12, compared with the much more rigid metal rotors could be an important reference in decision making for rotor model manufacture for performance testing. This paper presents the measured drag and power coefficients and comparison between these two sets of aircraft grade aluminium and sintered material similar to Nylon 12 [1]. A complete set of geometry and testing condition details and the design of fabrication of the test apparatus were also presented.

This paper aims to produce the following outcomes:

- To provide a complete set of measurement and geometry data for the two sets of bi-directional turbine rotor models for numerical code validation.
- To identify the cause of the hydrodynamic performance degradation of the plastic rotors by analysing the local flow condition of the blade sections.
- To shed some light on stall caused performance reduction due to flexibility of nylon materials and the selection of materials of rotors for

propulsion and energy generation in model design, manufacture, and testing.

1.1. The Rotor Models

As part of a larger research program, the authors developed a systematic series of ten different rotor models [12]. The test program was conducted in two phases. Phase 1 identified the effect of pitch, pitch distribution, solidity and Reynolds numbers on the power generation performance of seven rotors in this series, all fabricated of metal (aircraft grade aluminium), as reported in [13]. As previously mentioned, an aim of the present study (Phase 2) is to identify and compare the performance of metal and plastic rotors, whereby further experiments were performed on two of the seven rotors previously published [13].

There was a consideration to avail of the possibility of testing at the Cavitation Tunnel at the National Research Council Canada (NRC) St. John's. The test section of the NRC cavitation tunnel is $0.5m \times 0.5m$. The diameter of the rotors were limited to around 200 mm by the current technology of the selective laser sintering (SLS) systems, so called 3D printers at the time when they were made (around 2010). Based on these limitations, the diameter of the rotors was taken as 0.23 m. The two plastic rotors were produced by an SLS system, i.e., a 3D printer, made of polyamide (similar to Nylon 12) material. The rated ultimate tensile strength of the polyamide is 43 MPa but the rigidity is rather low with that much tensile strength. To increase the rigidity, rotor blade sectional thickness was increased by 50% compared with the full scale (20m diameter) for both plastic and metal rotors to maintain the same design hydrodynamic characteristics of the blade sections. The two metal rotors were made using computer numerical control (CNC) of aircraft grade aluminium (6061 series) by Danford Engineering, Victoria, Australia. The two plastic rotors were made at Memorial University of Newfoundland along with other 8 plastic rotors. These two plastic rotors presented in this work have the identical geometry of the corresponding metal rotors.

Table 2 lists the key geometry parameters of the rotor model sets. The pitch ratio is measured at 0.7R and D_h/D is the ratio of the hub diameter to rotor diameter.

Table 2: Key geometry parameters of the rotors

Rotor No.	$D_m(m)$	p_D	EAR	D_h/D
2	0.23	0.31	0.80	0.15
3	0.23	0.27	0.80	0.15

The detailed planform geometry and blade sectional offsets of these 2 sets of rotor models, as part of the input file for the panel method code, Propella [11], used for numerical simulation and optimization are provided in full in [13].

The solidity EAR of these rotors are very large ($EAR = 0.8$). Earlier design and optimization work completed numerically and presented in [12] developed a series of ten rotors in which EAR ranges from 0.4 to 0.8. To perform a fair and accurate comparison between the plastic and metal rotors, the geometry and the testing conditions of the corresponding rotors must be the same. In model testing to obtain a relatively large Reynolds number in order to minimize or eliminate Reynolds effect, the 0.23 m rotors must rotate fast with a fast inflow speed so this in combination will produce a large Reynolds number and desired TSR. However, plastic rotors with a small EAR have poor strength and an inability to cope with the high rotation speed and fast inflow speed. Therefore, only the plastic rotors with the largest EAR of 0.8 were tested.

Figure 1 show the surface mesh and the metal rotor models. As it can be seen in Table 2, rotors no. 2 and 3 have the same solidity, diameter, and hub diameter, but vary slightly in pitch ratio.

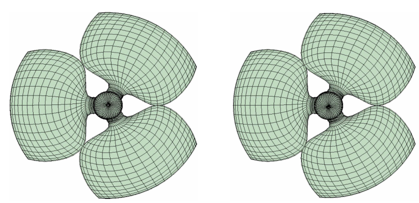

(a) Rotor No. 2 (b) Rotor No. 3

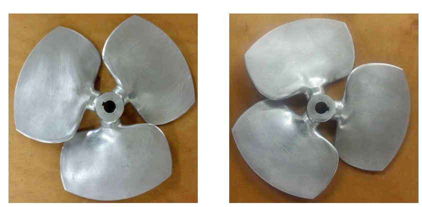

(c) Rotor No. 2 (d) Rotor No. 3

Figure 1: Metal rotors No. 2 and 3

The root sections were designed to be perfectly circular, because other sectional shape at the very small radius locations were deemed to contribute more drag than power. Circular root sections will have a uniform strength in any bending direction (spindle torque, in-plane and out-of-plane bending moment — for detail, see [15]). The circular root section and a small hub diameter in combination will save materials as well, if the full scale rotor hub is designed and made from a billet of material.

Numerically, the surface mesh generated by code Propella at the blade root requires pitch alignment so the root sections had a very large pitch to obtain a perfect connection between the adjacent panels on the hub and blade root. The code requires nearly the same local panel corner point coordinates ($1.0E10^{-8}$ in error) as the coordinates of the neighbour panels to determine the adjacent panels and thus to obtain the doublet velocity potential by taking finite difference derivatives across the neighbour panels on both hub and blade root. As the first 7 blade sections are all circular, their pitch value does not affect the performance of the rotor. Streamline sections start at the 8th section, at $r/R = 0.2$. This means that if the hub diameter ratio increases from 0.15 to 0.2, except for little difference in drag (added drag due to a larger hub diameter), power performance of the rotor will basically remain unchanged.

Figure 2 shows the plastic rotors No. 2 and 3.

In the code Propella, a two-way spline scheme for the blade surface contour was established [9] and used to interpolate and generate the blade surface, in terms of a prescribed number of chordwise and spanwise intervals in the input file for the code to generate rotor surface panels.

2. Test Apparatus, Calibration and Setup

2.1. Test Apparatus

A new rotor testing apparatus was specially designed and built. Only a very brief introduction to the structure, configuration and setup of the

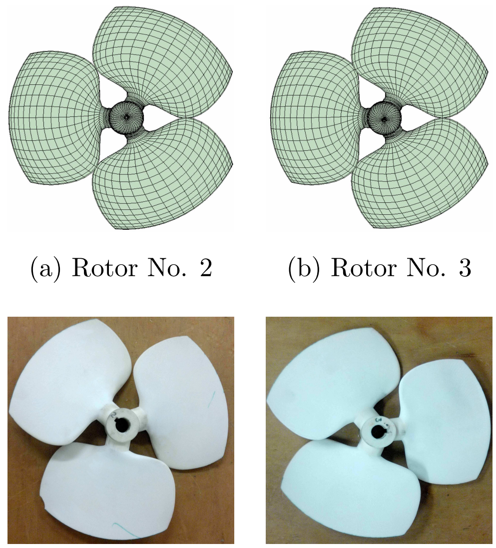

(a) Rotor No. 2 (b) Rotor No. 3

(c) Rotor No. 2 (d) Rotor No. 3

Figure 2: Plastic rotors No. 2 and 3

apparatus is given here.

Figure 3 shows the internal assembly and individual components of the opensboat for this work.

In figure 3, from bottom to top, is the nylon seat (in figure 3b) to provide a floating mount with torque and thrust retainer, the motor (in figure 3c), the universal shaft coupling, the K&R propeller dynamometer (in figure 3d), the end shaft coupling and drag retainer, and the cone cap (in figure 3e) of the opensboat casing.

The capacities of the R31 K&R dynamometer are 4 Nm torque and 100 N thrust/drag. It was the smallest K&R dynamometer among the 4 K&R dynamometers available at Australian Maritime College (AMC). As will be discussed in section 3, a smaller torque capacity of about 2 Nm and the

(a) Internal assembly

(b) Nylon seat

(c) BG 65 PI Motor

(d) K&R R31 dyno

(e) Cone cap

Figure 3: Internal assembly of the opensboat

same thrust capacity would be ideal for the rotor model working condition, controller ampere rating, motor shaft speed limit and the available carriage speed of the tow tank.

The motor used is a Dunkermotoren BG 65 PI. It has 2 sets of cable connections, the 12-pin and 5-pin ones [6]. The 12-pin connection is power signal cable for power and speed input and the 5-pin connection is service signal for PC. The motor gear box ratio is 3:1. Motor controller amperage rate is 8A. The motor shaft speed limit is 6000 RPM, so the maximum allowable rotor shaft speed is 2000 RPM, about 33 rps.

The control of the motor is realized by proprietary software that permits up to 8 speeds (2^3) prescribed on computer. These parameters of the 8 speeds are loaded in to the motor's circuity from the software. The speeds are obtained by sending a corresponding binary code to a stored speed, which are manually set in the GUI of the software on PC. A binary box was created by AMC and was used to send the binary code real time on the fly. The shaft speed, when no binary signal input, is also controlled at zero. The rotor shaft speed does not have an indexing feedback which would make more automation and efficiency in data acquisition and processing.

Figure 4 shows the opensboat assembly and its setup mounting on the carriage over the AMC towing tank.

(a) Opensboat assembly (b) Opensboat setup

Figure 4: Opensboat assembly and test setup

The casing of the opensboat is made of aircraft grade aluminium. The mid part of the casing is made of aluminium plate that was wrapped and welded together. The cone cap is a solid one-piece.

The two vertical tubes that supported the opensboat (seen in Figure 4a) were not covered with streamlined shells as planned. A substantial vortex induced vibration and transverse oscillation occurred at carriage speeds in excess of 2 m/s. The carriage speed was initially set to 1 m/s and no obvious vibration was noticed. However, to improve the accuracy of the measurements by increasing measured torque and hence torque sensitivity and reducing the Reynolds number effect, it was set at 1.5 m/s for most data points. A tension cable was applied to wrap around the mid part of the opensboat and be anchored across the mounting seat of the towing tank carriage. These significantly reduced traverse motion, vortex induced vibration and self-excitation.

The AMC towing tank is 100 m long, 3.5 m wide, 1.5 m deep. The maximum carriage speed of the towing tank is 4.6 m/s [2].

The rotor is placed upstream with a shaft immersion depth of 0.75 m (half tank depth) to reduce the free surface and bottom wall effect to minimum. The gondola (opensboat body) is about 5-diameter downstream of the rotor plane — the distance is far enough to reduce the effect on torque and hence power coefficient measurement on the rotor to the minimum, that could be possibly created by the interaction between the shed vortices and the gondola body.

2.2. Dynamometer Calibration and Data Acquisition Setup

The most important hydrodynamic performance characteristics of a turbine rotor is its power coefficient versus tip speed ratio TSR. Another hydrodynamic property to measure is the drag/thrust coefficient. These coefficients and the TSR are, for turbine rotors, usually expressed as:

$$C_{pow} = \frac{Q \times \omega}{\frac{1}{2}\rho V^3 A}, \quad (1)$$

$$C_t = \frac{T}{\frac{1}{2}\rho V^2 A}, \quad (2)$$

and

$$TSR = \frac{\omega R}{V}, \quad (3)$$

where Q is rotor shaft torque in Nm, ω shaft revolution speed in rps, ρ fluid density in kg/m^3, V inflow speed in m/s, T the thrust/drag in N, A the rotor sweep area in m^2, and R the radius of the rotor, respectively.

For the testing measurement, there are three channels captured simultaneously for data acquisition, they are: carriage speed, drag/thrust and torque output. As mentioned previously, the shaft speed channel is separate as an individual channel that is controlled by the proprietary software. The shaft revolution speeds in RPM, rounded off from the 2nd decimal point of RPM (round off error at 1/120 rps), were pre-set on computer for each desired tip speed ratio. The carriage speeds, thrust and torque coefficients are actually measured values after applying the gain.

The averaged speed, drag/thrust and torque gains obtained are $g_a = 0.500$, 7.025 and 0.130, respectively and their offsets are nearly zero. Therefore, the measured value is $F = V_{measured}(g_a - 0.0)$.

A 32-channel PCI-6254M series data acquisition system by National Instruments is used. A 32-bit version 2010 Labview was used as the data acquisition software. The computer on the towing tank carriage used is an HP 8100 Elite Desktop with an Intel Core i5 650@3.2GHz CPU and 8 GB of RAM, running a 64-bit Win 7.

The sample rate for all data points is 1000 Hz which gives about 80 data points per revolution. For fast propeller testing, a much higher sample rate at 20 kHz is commonly used in practice but a much lower sample rate can also be found for wind turbine rotor testing at 20 Hz [3]. The sample rate of 1000 Hz for this testing program was deemed necessary and sufficiently high. At the beginning of the testing, a sample time of 20 seconds for a carriage speed of 1 m/s was used but it seemed unnecessarily long. Most of the data points were obtained using 10 seconds sample time at a carriage speed of 1.5 m/s. There are over 10000 samples over the 10-second period. Only 9500 samples are used to obtain the averaged measurement at each data point. Using a reduced sample time increased productivity of obtaining 2-3 data points over one carriage trip of about 80 metres long.

3. Results and Discussions

3.1. Tare thrust and torque to adjust measurements

For turbine rotor performance, accuracy of torque measurement is much more important than that of drag/thrust, while accuracy on thrust is the most important for propulsion tests for ship speed estimate. During the testing the maximum measured torque at a constant 1.5 m/s carriage speed is about 0.5 Nm and the tare (friction) torque is about 0.1 Nm. The tare torque relative to the capacity of 4 Nm is too small to eliminate sensitivity concern. After all the testing was completed, torque sensitivity was carefully verified and obtained for data correction/adjustment. During the test at the beginning and the end of each day, tare torques were measured at various possible shaft rotation speeds without the rotor. No dummy hub was used. The ITTC propulsion testing guidelines [7] and a wind turbine testing work [3] were used as reference for tare torque measurement and adjustment.

A set of extensive tare torque measurement runs were also conducted to examine tare variations with shaft speeds. Total of four ranges of shaft speeds were tested corresponding to the inflow speed of 1.5, 2.0, 2.5, and 3.0 m/s. Figure 5 shows the processed measurements. The sample rate and time were the same as rotor testing condition, i.e., 1000 Hz and 10 seconds, respectively.

Note that measurements shown in Figure 5 were obtained within one day. For the rotor shaft measured torque adjustment, tare torque values were obtained each day before the rotor measurement starts and the tare torque values in the morning were used in the adjustment. Tare torque values were also obtained after testing at the end of each day and were checked against these values obtained in the morning. No significant difference was found so all the measurements were adjusted using the tare torque values in each morning.

For turbine rotor torque measurement, the total rotor shaft torque for power generation calculation, were obtained by:

$$Q_{adj} \quad = \quad \pm Q_{tare} + Q_{measured} - Q_0, \tag{4}$$

where Q_{adj}, Q_{tare}, $Q_{measured}$ and Q_0 are adjusted torque measurement, tare torque, measured torque and torque reading at zero torque load. The sign of the Q_{tare} values should be taken to increase the absolute measured torque

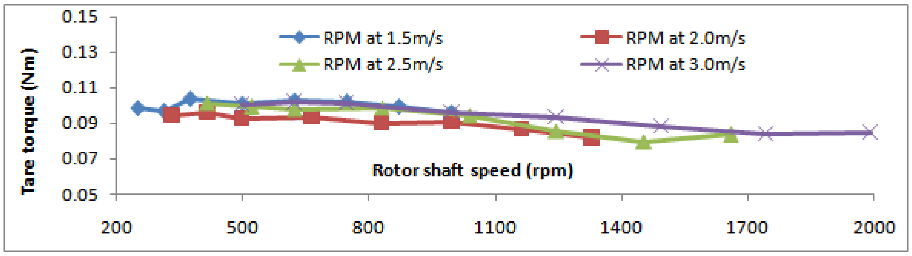

(a) Averaged tare torque (Nm) versus rotor shaft speed

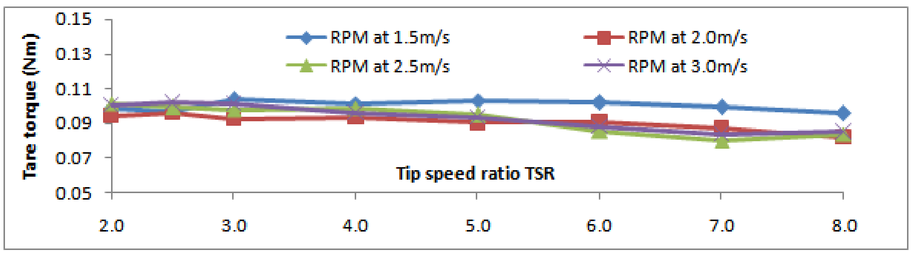

(b) Averaged tare torque (Nm) versus equavlent tip speed ratio TSR

Figure 5: Averaged tare torque versus shaft speeds and equivalent tip speed ratios TSR corresponding to an inflow speed of 1.5, 2.0, 2.5 and 3.0 m/s

values, for either propulsion (positive torque) or turbine (negative torque) mode.

For drag measurement, the total rotor shaft drag force for power generation calculation, were obtained by:

$$T_{adj} = \pm T_{tare} + T_{measured} - T_0, \tag{5}$$

where T_{adj}, T_{tare}, $T_{measured}$ and T_0 are adjusted drag/thrust measurement, tare drag/thrust, measured drag/thrust and drag/thrust reading at zero drag/thrust load. The sign of the T_{tare} values should be taken to increase the absolute measured drag/thrust values for both turbine and propulsion mode.

3.2. Test Matrix for Data Acquisition

The two sets of rotor models and the test matrix were designed to provide design reference on hydrodynamic performance characteristic of the bi-directional tidal turbine rotors and sufficient data for numerical codes validation. Even though drag measurements are not the most important for turbine rotor design, these measurements are very important for numerical codes to validate when both drag and torque are available the same time.

The initial plan was to obtain thrust and power coefficient for each rotor versus a range of tip speed ratio TSR from 2.0 to 8.0. After a series of testing runs, it was found that most power coefficient measured at a TSR greater than 6.0 are negative so any power coefficient at $TSR > 6.0$ is not meaningful. Table 3 shows the required shaft speeds corresponding to the pre-set TSR for all the rotors of D=0.23 m, under an inflow speed (carriage speed) of 1.5 m/s.

Table 3: TSR versus required shaft speed

TSR	6.00	5.00	4.00	3.00	2.50	2.00
n (rps)	12.5	10.4	8.3	6.2	5.2	4.2
N (RPM)	747.3	622.8	498.2	373.7	311.4	249.1

There are total of 6 TSR points and 4 (2 aluminium and 2 nylon) rotors so the minimum required number of total data points runs is 24. With the calibration runs, tare runs and some trial runs, the number of total runs for both first and second phase of the testing program exceeded 300.

3.3. Power and Drag Performance comparison

Figures 6 and 7 show drag and power coefficients of the two set of rotors with the same geometry.

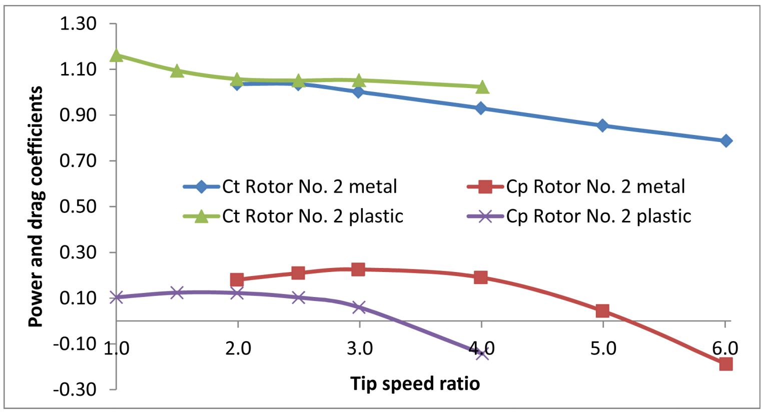

Figure 6: Effect of flexibility and surface roughness on drag and power coefficients, metal versus plastic of Rotor No. 2

It can be seen for both rotor No. 2 and 3 that the drag coefficient of the plastic rotors are just slightly higher than the metal rotors throughout the TSR range, with a slight increase when the inflow speed becomes large at a tip speed ratio (TSR) greater than 2.5. The increased drag of the plastic rotors is caused by rougher blade surfaces and hence larger skin friction.

The maximum power coefficient however, produced by the plastic rotors is about only 60% of the metal ones. The plastic rotors at a TSR of greater than 3.2 (Rotor No. 3) and 3.3 (No. 2) start to produce negative power. The much reduced power production of the plastic rotors is mainly due to the flexibility that caused a change in effective angle of attack (or effective pitch) of the blade sections. It can be seen also that the plastic rotors' cut-in speed, the minimum inflow speed required to turn the rotor, is much higher

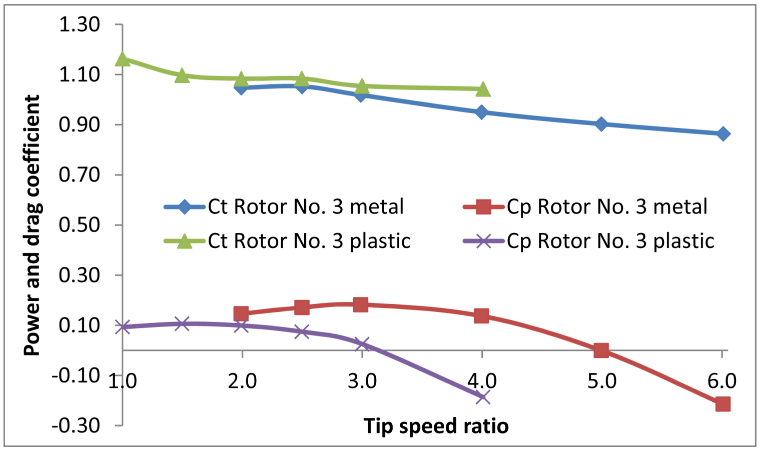

Figure 7: Effect of flexibility and surface roughness on drag and power coefficients of Rotor No. 3

than the metal ones — TSR is proportional to the inverse of the inflow velocity. The effect of flexibility on peak power coefficients and cut-in speed, is discussed in the following section.

3.4. Power Performance Analysis

The dramatic decrease in power coefficient of the rotor made from plastic material is caused by flexibility and the change in effective pitch of the sections. The substantially increased cut-in speed, i.e., the inability to generate power at low speed current becomes significant compared with the metal ones: power coefficient falls to zero at $TSR \sim 3.2$ (Rotor No. 3) and $TSR \sim 3.3$ (No. 2) for plastic rotors and $TSR \sim 5.2$ (Rotor No. 2) and $TSR \sim 5.0$ (No. 3) for metal ones, as shown in Figures 6 and 7. However, at a very low TSR of about 1.0 of which the inflow velocity at maximum, the plastic rotors can still generate positive power but the metal rotors already generate negative power (by extrapolating the power coefficient curves to the left).

As mentioned, all the blade sections of the bi-directional rotor are fully symmetrical. What is the change in pitch, is it increased or decreased, and how is it changed, due to the flexibility of the plastic material? To find answers to the above questions, a velocity diagram for a flexible blade section to determine the effective angle of attack, resulted in a combination of the blade sectional geometrical pitch, camber, and inflow velocity, similar to a rigid foil section presented by Liu [10], is shown in figure 8.

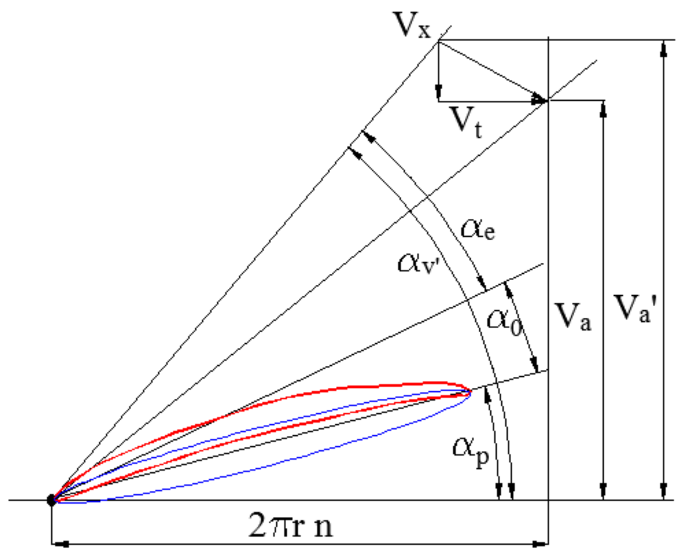

Figure 8: Effective angle of attack velocity diagram of a flexible turbine rotor blade section

Variables in Figure 8, have been defined in the nomenclature.

Due to flexibility, the rigid foil section (in blue) is bent back as it faces the inflow, similar to a circular arc section (in red). This increases the camber of the foil section and hence increases the angle of zero lift, α_o. Normally the higher the flexibility, the larger the deflection. As the foil section is fully symmetrical, the initial angle of zero lift is zero. The effective angle of attack of the foil section can be expressed as:

$$\alpha_e = \alpha_{v'} + \alpha_o - \alpha_p \quad (6)$$

Equation 6 shows that the larger the negative value of the angle of zero lift α_o, the more reduction of the effective angle of attack α_e. Due to flexibility of the plastic rotors, the more deflection of the blade section the larger the negative angle of zero lift. Normally for turbine rotors below the stall region, the lower the pitch, the higher the effective angle of attack (opposite to a propeller blade section which the higher the pitch the lower the effective angle of attack), and hence the higher the power coefficient. The only reason for the plastic rotors to produce an increased power coefficient when effective angle of attack decreases, is that the reduction in the effective angle of attack has retarded the severe stall. As is known, stall starts at a sufficiently large effective angle of attack under a small enough Reynolds number. For example, stall occurs at $\alpha_e > 12°$ for a 2D NACA 0012 foil at a Reynolds number of about 0.66 million and at $\alpha_e > 16°$ with a Reynolds number of about 3.18 million [8]. A substantial reduction in power coefficient suggests that at a very low TSR of about 1.0, the metal rotor sections are under severe stall but the plastic rotors still have a power coefficient at the same TSR. For turbine testing at constant shaft revolution speed, the lower the TSR, the higher the Reynolds number.

During phase I of the testing program [13], the effect of Reynolds number on the inflow speed was discussed and analysed in detail. The power coefficients for both Phase I and II were obtained at an inflow speed of 1.5

m/s for which Reynolds number has little influence on the accuracy of the measurement. For these plastic and metal rotors under consideration, at an inflow speed of 1.5 m/s, the Reynolds number calculated based on the 0.7R chord length, is 0.28 million at TSR =1.0 and 0.98 million at TSR=6.

To find out whether the blade sections are under severe stall, let's consider the foil tip section at $r = 1.0R$ at a TSR of 1.0 and ignore the induced velocity V_x and V_t. Thus the angle of inflow is:

$$\begin{aligned} tan(\alpha'_V) &= \frac{V'_a}{2\pi nR} = \frac{V'_a}{\pi nD} = \frac{1}{TSR} = 1. && (7) \\ \alpha'_V &= 45°. && (8) \end{aligned}$$

$$\begin{aligned} \alpha_p &= tan^{-1}\left(\frac{\frac{p}{D}nD}{2\pi nR}\right) = tan^{-1}\left(\frac{\frac{p}{D}}{\pi}\right), && (9) \\ \alpha_{p_{31}} &= tan^{-1}\left(\frac{0.31}{\pi}\right) = 5.6°, && (10) \\ \alpha_{p_{27}} &= tan^{-1}\left(\frac{0.27}{\pi}\right) = 4.9°. && (11) \end{aligned}$$

For the rigid and fully symmetrical blade section, the angle of zero lift of metal rotors is zero. The effective angles of attack for the metal rotors no. 2 and 3 at the blade tip section, assuming a zero chordwise flexibility, are then:

$$\begin{aligned} \alpha_{e_{27}} &= \alpha'_{v_{27}} + \alpha_{o_{27}} - \alpha_{p_{27}} = 45 + 0.0 - 4.9 = 40.1° && (12) \\ \alpha_{e_{31}} &= \alpha'_{v_{31}} + \alpha_{o_{31}} - \alpha_{p_{31}} = 45 + 0.0 - 5.6 = 39.4° && (13) \end{aligned}$$

The aspect ratio of a rotor blade is semi infinite if the hub at the blade root is assumed an infinitely large wall. At an effective angle of attack of about 40° at a Reynolds number of 0.28 million, the blade section of the metal rotor with a semi infinite aspect ratio has no doubt a severe stall. A reduction of the effective angle of attack will then retard or avoid the severe stall and hence improve the performance of the power generation performance.

For the plastic rotors, the angle of zero lift due to the deformation of the blade section could be estimated approximately using the expression suggested by Marchaj [16] as:

$$\alpha_o = -360°(\frac{f}{c}). \tag{14}$$

For the soft and flexible blade section of the plastic rotors facing a 1.5 m/s inflow, a bent chord section resulted in a camber of about 20% chord length, estimated based on the amount of deformation tested in the air by pressing the blade edges, will result in an angle of zero lift of about -23° for a 2D foil. The effective angles of attack of the plastic foils are therefore about 20° less than the metal ones, at about 25°. This value of the effective angle of attack has much less stall than the metals at about 40°. This implies that a chordwise flexible blade section can reduce the effective angle of attack and hence retard severe stall, especially at a very large inflow speed when the rotor encounters a gust current or wind in a harsh environment.

The power coefficient of these metal rotors are relatively small (0.22) because their large solidity of $EAR = 0.8$ and the bi-directional blade section (full symmetrical, i.e., zero camber and identical L.E. and T.E. profiles). If the blade section is designed as a unidirectional profile with a much higher camber and hence lift, its power coefficient C_{pow} could be much higher (0.3-0.4 or even higher). The higher the lift of a wing section, the higher the pitching moment of the wing. If the same plastic material is used for a rotor with a high camber profile section and hence a much higher power coefficient around 0.4, the performance reduction due to the very softness and high flexibility of the plastic material is expected to be similar, unless the plastic rotor blade section is made much thicker, say, 2 or 3 times as thick.

For marine propellers, the angle of zero lift decreases (becomes less negative) due to the blade chordwise flexibility —blade section bent in an opposite direction of turbine rotors. This ends up a reduction of the resultant effective angle of attack at the propeller blade section. Under a very heave load condition, chordwise deflection becomes large to result in a substantially reduced effective angle of attack and hence reduces the possibility of stall and cavitation. As a result, a flexible propeller blade section will produce a less thrust production than rigid rotors in medium and light load conditions.

4. Conclusions and Recommendations

Experimental tests were conducted to evaluate the performance of two sets of metal and plastic bi-directional tidal turbine rotor models. Comparison between the metal and plastic rotors hydrodynamic performance in terms of torque, drag and derived power and drag coefficients were obtained and are presented. The results show a substantial decrease in maximum power performance for the plastic rotors — about 40% decrease at a tip speed ratio of around 3.0 compared with the metal rotors. The plastic rotors operate in a much smaller TSR range and hence a much larger cut-in speed. The main reason for the reduction in power performance of the plastic rotors was found to be the change in angle of zero lift because of the bending of the blade section due to flexibility. The change in zero lift reduces the effective angle of attack. It is concluded that materials for rotor models with poor rigidity such as polyamide (nylon) produced by selective laser sintering (SLS) systems, are not suitable for rotor model performance evaluation.

The comparison of performance between the metal and nylon rotors indicates that the plastic rotors have a significantly reduced power output (40% less than the metal ones) mainly due to flexibility of the soft material used. The flexibility of the chordwise blade section increases the negative value of the angle of zero lift and hence decreases the effective angle of attack, from about 40° to about 25° at the tip section at a Reynolds number of 0.28 million, as an example estimation. The change in angle of zero of lift due to flexibility substantially reduced the effective angle of attack has avoided a severe stall and hence improved the power performance at a very large inflow speed (very low TSR of about 1.0).

Acknowledgement

The authors would like to acknowledge the following organizations and individuals:

- University of Tasmania for the Visiting Fellow award to the first author and financial support for the testing program;
- National Research Council Canada (NRC) for initial and continued support to this renewable energy project;
- NRC colleagues Scott Reid and Tom Hall for rotor design and fabrication support, and Rob Pallard and Darrell Sparkes for their valuable tips and values for tare torque measurements;

- AMC-UTAS colleagues Liam Honeychurch and Kirk Meyer for fabrication, setup and testing support at the Tow Tank at AMC-UTAS; and

- Graduate student Nick Osborne, under a joint graduate program between AMC-UTAS, Australia and Dalhousie University, Canada for his assistance during the testing.

Appendix A. Data in Tables

The following are the 4 tables that contain the measurement and analysed data for the two sets of rotors. Note that the values of drag T in Newtons and coefficient C_t should be **doubled** because the drag/thrust gain was tuned to half, listed in this appendix.

Table A.4: Measurement data for metal rotor No. 2

Rotor No. 2, $P_{D_{07R}}$=0.31, $P_{D_{tip}}$=0.31, EAR=0.80												
	Measured data				Tare Data			Net Outputs				
Run	N (RPM)	Vin	T (N))	Q (Nm)	T (N))	Q (Nm)	TSR	T (N))	Q (Nm)	P (W)	Ct 2	Cp 2
201	249	1.5066	22.63	-0.4023	-1.79	0.0886	1.991	24.42	0.4909	12.805	0.5178	0.1802
201_2	311	1.5035	22.52	-0.3605	-1.78	0.0921	2.494	24.30	0.4526	14.758	0.5175	0.2090
202	374	1.5059	21.82	-0.3140	-1.78	0.0946	2.988	23.60	0.4086	15.989	0.5009	0.2254
202_2	498	1.5023	20.03	-0.1561	-1.77	0.1010	3.994	21.80	0.2571	13.411	0.4650	0.1904
203	623	1.5018	18.25	0.0482	-1.76	0.0957	4.994	20.01	0.0475	3.097	0.4271	0.0440
203_2	747	1.4979	16.61	0.2576	-1.73	0.0899	6.008	18.35	-0.1677	-13.124	0.3936	-0.1880

References

[1] 3DSystems, 21 Nov 2006. Duraform plastic for use with all selective laser sintering (sls) systems. Tech. Rep. PN 70715, 3D Systems.

Table A.5: Measurement data for metal rotor No. 3

Rotor No. 3, $P_{D_{07R}}$=0.27, $P_{D_{tip}}$=0.27, EAR=0.80												
	Measured data				Tare Data			Net Outputs				
Run	N (RPM)	Vin	T (N))	Q (Nm)	T (N))	Q (Nm)	TSR	T (N))	Q (Nm)	P (W)	Ct 3	Cp 3
207	249	1.5058	22.88	-0.3092	-1.79	0.0886	1.992	24.67	0.3978	10.377	0.5238	0.1463
207_2	311	1.5011	22.86	-0.2773	-1.78	0.0921	2.498	24.64	0.3694	12.044	0.5264	0.1714
208	374	1.5059	22.21	-0.2363	-1.78	0.0946	2.988	23.99	0.3309	12.948	0.5092	0.1825
208_2	498	1.5018	20.49	-0.0843	-1.77	0.1010	3.995	22.26	0.1852	9.664	0.4751	0.1374
209	623	1.5016	19.38	0.0963	-1.76	0.0957	4.995	21.14	-0.0006	-0.038	0.4514	-0.0005
209_2	747	1.4971	18.38	0.2811	-1.73	0.0899	6.011	20.12	-0.1912	-14.961	0.4320	-0.2146

Table A.6: Measurement data for plastic rotor No. 2

Rotor No. 2 Plastic, $P_{D_{07R}}$=0.31, $P_{D_{tip}}$=0.31, EAR=0.80												
	Measured data				Tare Data			Net Outputs				
Run	N (RPM)	Vin	T (N))	Q (Nm)	T (N))	Q (Nm)	TSR	T (N))	Q (Nm)	P (W)	Ct 2*	Cp 2*
228	125	1.5052	25.54	-0.4644	-1.80	0.0965	1.000	27.35	0.5609	7.342	0.5810	0.1036
228_2	187	1.502	23.83	-0.3487	-1.80	0.0965	1.499	25.63	0.4452	8.718	0.5470	0.1239
226	249	1.5059	23.10	-0.2376	-1.80	0.0949	1.992	24.91	0.3326	8.676	0.5288	0.1223
226_2	311	1.5020	22.83	-0.1237	-1.80	0.0980	2.497	24.64	0.2217	7.230	0.5256	0.1027
227	374	1.5039	22.92	-0.0066	-1.80	0.1020	2.992	24.72	0.1086	4.251	0.5261	0.0602
227_2	498	1.4975	22.04	0.2989	-1.80	0.1078	4.007	23.84	-0.1911	-9.969	0.5117	-0.1429

Table A.7: Measurement data for plastic rotor No. 3

Rotor No. 3 Plastic, $P_{D_{07R}}$=0.27, $P_{D_{tip}}$=0.27, EAR=0.80												
	Measured data				Tare Data			Net Outputs				
Run	N (RPM)	Vin	T (N))	Q (Nm)	T (N))	Q (Nm)	TSR	T (N))	Q (Nm)	P (W)	Ct 3*	Cp 3*
229	125	1.5050	25.57	-0.4081	-1.80	0.0965	1.000	27.37	0.5046	6.605	0.5817	0.0933
229_2	187	1.5029	23.94	-0.2856	-1.80	0.0965	1.498	25.74	0.3821	7.482	0.5487	0.1061
230	249	1.5055	23.71	-0.1748	-1.80	0.0949	1.993	25.52	0.2698	7.038	0.5419	0.0993
230_2	311	1.5015	23.58	-0.0628	-1.80	0.0980	2.498	25.38	0.1608	5.244	0.5420	0.0746
231	374	1.5002	22.85	0.0563	-1.80	0.1020	3.000	24.65	0.0457	1.788	0.5272	0.0255
231_2	498	1.497	22.48	0.3561	-1.80	0.1078	4.008	24.28	-0.2483	-12.952	0.5214	-0.1858

[2] AMC, Last visited in June 2015. Amc tow tank website. URL http://www.amc.edu.au/maritime-engineering/towing-tank

[3] Ashwill, T., July 1992. Measured data for the sandia 34-meter vertical axis turbine. Tech. Rep. SAND91-2228, Sandia National Laboratories.

[4] Bahaj, A., Batten, W., McCann, G., 2007. Power and thrust measurement of marine current turbines under various hydrodynamic flow conditions in a cavitation tunnel and a towing tank. Renewable Energy 32, 407–426.

[5] Butterfield, C., Musial, W., Simms, D., August 1992. Combined experiment phase i final report. Tech. Rep. NREL TP-257-4655, National Renewable Energy Laboratory.

[6] Dunkermotoren, Last visited in June 2015. Brushless dc-motors. URL http://www.dunkermotor.com

[7] ITTC, 2002. Testing and extrapolation methods: propulsion, performance propulsion test. Tech. Rep. 7.5-02-03-01.1, Internatonal Towing Tank Conference.

[8] Katz, J., Plotkin, A., 1991. Low-Speed Aerodynamic — From Wing Theory to Panel Methods. McGraw-Hill, Inc., New York.

[9] Liu, P., 1996. A time-domain panel method for oscillating propulsors with both spanwise and chordwise flexibility. Ph.D. thesis, Memorial University of Newfoundland.

[10] Liu, P., 2010. A computational hydrodynamics method for horizontal axis turbine — panel method modeling migration from propeller to turbine. Energy 35, 2843–2851.

[11] Liu, P., Bose, N., April 1998. An unsteady panel method for hihgly skewed propellers in non-uniform inflow. In: Gindroz, B., Hoshino, T., Pyllkanen, J. (Eds.), Propeller RANS/Panel Method Workshop, Grenoble, France. ITTC, pp. 343–350.

[12] Liu, P., Bose, N., 2012. Prototyping a series of bi-directional horizontal axis tidal turbines for optimum energy conversion. Applied Energy 99, 50–66.

[13] Liu, P., Bose, N., Frost, R., Macfarlane, G., Lilienthal, T., Penesis, I., Windsor, F., Thomas, G., 2014. Model testing of a series of bi-directional tidal turbine rotors. Energy 67, 397–410.
URL `http://dx.doi.org/10.1016/j.energy.2013.12.058`

[14] Liu, P., Bose, N., Frost, R., Macfarlane, G., Lilienthal, T., Penesis, I., Windsor, F., Thomas, G., July 2013. Model testing of a series of bi-directional current turbine rotors. Tech. Rep. OCRE-TR-2013-034, Protected B, OCRE-NRC Internal Report, OCRE, National Research Council Canada.

[15] Liu, P., Veitch, B., 2012. Design and optimization for strength and integrity of tidal turbine rotor blades. Energy 46, 392–404.

[16] Marchaj, C., 1988. Aero-hydrodynamics of Sailing. McGraw-Hill Trade, New York.